

NASA's advanced solar sail propulsion system for low-cost deep space exploration and science missions that uses high performance rollable composite booms

By Juan M. FERNANDEZ¹⁾, Geoffrey, K. ROSE¹⁾, Casey J. YOUNGER²⁾, Gregory D. DEAN¹⁾,
Jerry E. WARREN¹⁾, Olive R. STOHLMAN¹⁾, and W. Keats WILKIE¹⁾.

1) NASA Langley Research Center, Structural Dynamics Branch, Hampton, VA 23681, USA.

2) NASA Langley Research Center, Systems Integration and Test Branch, Hampton, VA 23681, USA.

juan.m.fernandez@nasa.gov

Several low-cost solar sail technology demonstrator missions are under development in the United States. However, the mass saving derived benefits that composites can offer to such a mass critical spacecraft architecture have not been realized yet. This is due to the lack of suitable composite booms that can fit inside CubeSat platforms and ultimately be readily scalable to much larger sizes, where they can fully optimize their use. With this aim, a new effort focused at developing scalable rollable composite booms for solar sails and other deployable structures has begun. Seven meter booms used to deploy a 90 m² class solar sail that can fit inside a 6U CubeSat have already been developed. The NASA road map to low-cost solar sail capability demonstration envisioned, consists of increasing the size of these composite booms to enable sailcrafts with a reflective area of up to 2000 m² housed aboard small satellite platforms. This paper presents a solar sail system initially conceived to serve as a risk reduction alternative to Near Earth Asteroid (NEA) Scout's baseline design but that has recently been slightly redesigned and proposed for follow-on missions. The features of the booms and various deployment mechanisms for the booms and sail, as well as ground support equipment used during testing, are introduced. The results of structural analyses predict the performance of the system under microgravity conditions. Finally, the results of the functional and environmental testing campaign carried out are shown.

Key Words: Solar Sails, Composite booms, Deployment Mechanisms, Functional and Environmental Testing.

1. Introduction

American low-cost CubeSat-based solar sail technology demonstrator missions are using metallic rollable booms as the deployable supporting structure for the sails. After the launch of NanoSail-D2¹⁾ and Lightsail 1²⁾, which demonstrated deployment of relatively small size solar sails, the two upcoming missions Lightsail 2³⁾ and National Aeronautics and Space Administration's (NASA) NEA Scout⁴⁾ will still rely on the same Elgiloy Triangular And Collapsible (TRAC) boom technology.⁵⁾ However, recent detailed thermo-structural analyses have shown the challenges that these booms, which have a high coefficient of thermal expansion (CTE)⁶⁾, can impose to the mission architecture. For example, NEA Scout had to switch from its initial optimal four-quadrant sail configuration to a single-square sail design supported only at its four vertices, in order to shade the metallic booms and reduce their thermally induced deflections to comfortable levels.

NASA Langley Research Center (LaRC) is developing part of the next generation of solar sail technology for small interplanetary spacecraft, with the aim of rapidly infusing it onto an existing exploration or science mission and/or proposing new ones with it. LaRC has developed and tested an Engineering Development Unit (EDU) of a 9.5 m by 9.5 m solar sail system that fits inside a 3U volume (length = 20 cm, width = 10 cm, height = 15 cm), and can be integrated into a larger CubeSat (i.e., 6U, 12U) or satellite. The sail is supported by four 7 m lenticular composite booms that are thermally stable with a near zero coefficient of thermal expansion in the boom axial direction. These high performance booms are made from state-of-the-art ultrathin carbon fiber materials that enable multi-directional laminates designed to balance challenging and conflicting requirements of the stored and deployed boom

configurations. Their lightweight design of only 16.5 g/m could save over 10% of the total spacecraft mass of proposed 6U CubeSat solar sail missions, resulting in more capable, faster and more agile solar sails. Current research is addressing the long-duration storage effects on the boom.

The boom deployer has an innovative design that increases deployment reliability by minimizing the risks of boom coil "blossoming", boom root buckling, and potential jamming during deployment, which has been observed on previous boom deployer concepts for similar applications.

The paper will present the design of the new composite boom concept, as well as the features and key components of the various deployment mechanisms for the booms and sail. An integrated boom-sail structural analysis will then be presented, showing the expected structural performance of the solar sail under microgravity conditions. The paper will finish with a summary of the functional and environmental testing campaign successfully completed on the solar sail system. This includes many full-scale ambient deployments, launch vibration tests, and partial boom-only deployments inside a thermal-vacuum chamber.

2. Composite Booms

Several new rollable composite boom concepts have been developed in accordance with NEA Scout's solar sail subsystem challenging requirements. These are presented in detail in 7). The boom with the highest structural performance was chosen for fabrication to the full-scale 6.85 m lengths required. This boom is a composite version of the so-called Collapsible Tubular Mast (CTM)⁸⁾, similar to what DLR has been producing for solar sails^{9,10)}, but using thin-ply spread-tow composite materials that enable a much smaller boom cross-section design. The flattened/stowed height of these carbon fiber reinforced

plastic (CFRP) Mini-CTM or Omega booms is just 45 mm. The two-ply [± 45 PW/0] non-symmetric lay-up adopted was chosen to comply with the volume requirements of the stored configuration and the structural requirements of the deployed one. The shell structure walls are 0.115 mm thick, and the thicker bonded edges are about 0.33 mm. The booms have a computed near zero axial CTE of $\alpha_{CTE,11} = -0.07$ ppm/ $^{\circ}$ C, making them practically inert to environmental extreme thermal condition fluctuations. The boom linear density is 16.5 g/m, so the four full-scale booms only weigh 452 g.

Boom fabrication with carbon foam molds yield a repeatable process that produces near perfectly straight booms over 7 m lengths, as shown in Fig. 1 (a), with only sub-centimeter errors. Measurements of the boom cross-section, taken before and after the EDU testing campaign, have shown that the boom material will be subjected to significant creep effects during long-term stowage, that ultimately yields a non-recoverable flattened cross-section with a reduced subtended angle, α . This affects the weaker in-plane moment of area, I_{yy} , of the boom, lowering its buckling load. The booms tested had an as-manufactured $\alpha = 80^{\circ}$ (see Fig. 1 (b)), but the highly-strained critical root sections experienced a subtended angle reduction of up to 30° after prolonged stowage, bringing them close to the lower limit of the acceptable range, as hinted in Fig. 2.

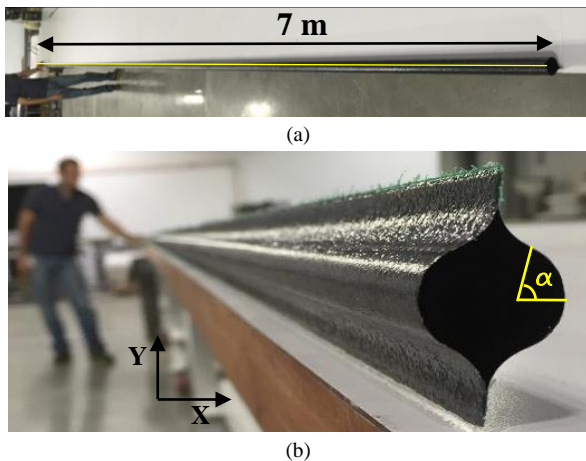


Fig. 1. (a) Near perfectly-straight 7 m boom; (b) Cross-section before being rolled, showing the subtended angle, α .

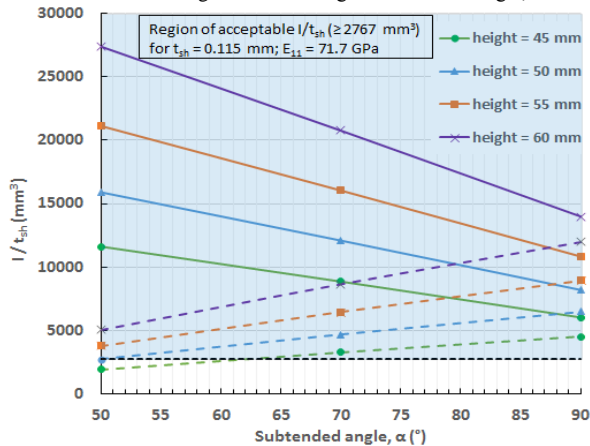


Fig. 2. Moment of area, I , divided by the boom wall thickness, t_{sh} , in both principal boom directions, x (solid line) and y (dashed line), as a function of the cross-section subtended angle, α , for different boom stowed height designs, h . The black dotted line marks the acceptable threshold following the boom bending stiffness ($E_{11}I$) requirements.

3. Solar Sail Deployment Mechanisms

One of the biggest challenges of rollable booms is managing the coil, such that during deployment it behaves like a solid with all coiled sections rotating in unison. Failing to do so, results in an unpredictable phenomenon called “blossoming”, where the outer layers move relative to the inner ones, posing the ultimate risk of deployment failure or boom damage.¹¹ Traditional boom deployers for CubeSats have used a simple “pusher” type concept, where the boom hubs are mechanically coupled to the motor, and thus, the boom extension force is of a pusher nature.¹² Such an approach promotes blossoming and it needs to be carefully managed by constraining the coil radially at multiple locations, which is not always possible in volume constrained CubeSat designs, or by partial retraction during boom deployment to tighten the coil.^{13, 14} However, accurate knowledge of the boom length extension, when multiple in and out cycles are imposed, becomes another challenge in itself.

Herein, a new “puller” type design, based on DeorbitSail’s boom deployer concept^{15,16}, was adopted. Fig. 3 shows a rendering of the complete Composites-based Solar Sail System (CS3) developed, including the boom deployer in question. In this so-called “puller” concept, a single central motor (A) pulls the four booms (B) out, by simultaneously reeling onto a central spool two thin Steel strips (C), each of which is secured to one of the two boom hubs/spools (D), and that initially get co-wrapped with the booms during stowage. A power spring (E) inside the boom spool maintains strip tension and external pressure on the boom coil throughout deployment. The strip tension and the moment arm to the outer perimeter of the boom coil provide the necessary moment to rotate each boom hub on thin-section bearings housed on the top and bottom aluminum plates of the boom deployer (M).

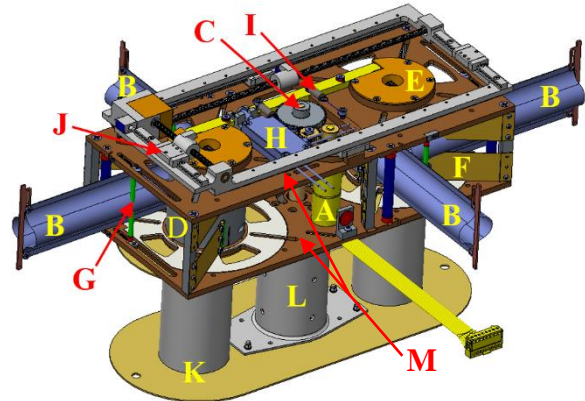


Fig. 3. Components of the CS3 initially developed for the NEA Scout mission. A: Motor; B: Booms; C: Steel strips spool’s gear; D: Boom spool; E: Encoder and power springs hubs; F: Spring arms; G: Sliding roller; H: Pin pusher/puller; I: Launch lock bar; J: AMT unit; K: Single-sail spool; L: Sail post (inside); M: Boom deployer top and bottom plates.

The unit has compliant radial spring arms (F) anchored to the boom deployer standoffs. The spring arms are made from thin metallic sheeting for a compact design, with end rollers that provide additional constraining forces to the boom coils during deployment and contact support near the

attachment points after deployment. Also, a series of fixed and spring-loaded sliding rollers (G) provide lateral support to the booms away from its clamped root. The boom hubs have omega-shaped cut-out sections and spring-slider connections for boom attachment to facilitate full recovery of the boom cross-section once completely deployed. A miniature pin pusher/puller (G), custom-made by Glenair Inc.,¹ fixed to a long lock/release bar mechanism (H) engages cog features on the two boom spools and the Steel strips spool. This is used as a launch lock system and after the booms are deployed to prevent further spool rotation.

In order to provide attitude control to the sailcraft, a two-axis active mass translation system (AMT), that follows the same center of pressure to center of mass (CP-CM) offset method to that of the Surrey Space Center's Translation Stage Unit (TSU) for CubeSail^{17,18}, has been developed by NASA Marshall Space Flight Center (MSFC). This is shown as (J) on Fig. 3. It will allow relative planar movement between the top and bottom halves of the spacecraft to provide the necessary trimming of the sail.

The single-sail spool (K) design depicted in Fig. 3 corresponds to the one from NEA Scout's single-square sail configuration. This oval-shaped spool will rotate with respect to the fixed inner sail post (L) to unfurl the sail membrane. In this configuration, the single-square sail is only supported at its four vertices and tensioned through linear springs connected to the four boom tips. However, the new Advanced Composites-based Solar Sail System (ACS3) design proposed herein, uses a four-quadrant sail configuration, as originally intended for NEA Scout, which generates less asymmetric boom loads during deployment with a more deterministic load path. Fig. 4 shows the twin-spool design adopted, where two quadrants are Z-folded along one direction and wrapped around each sail spool for stowage. A central post still provides structural support and serves as a cable feed-through port. Each triangular sail quadrant will be supported from its two adjacent boom tips and tensioned at the vertex near the spacecraft by a purposely-designed retractable lanyard unit (C). This will use a power/clock spring that sits below the sail spools and provides a nearly constant force independent of spring deflection and changing environmental conditions. Both the lanyards and the sail spools are allowed to rotate while the sail is unfurling, but towards the end of deployment, the lanyards leave the sail spool slots and finally lock into position when the quadrants are tensioned.

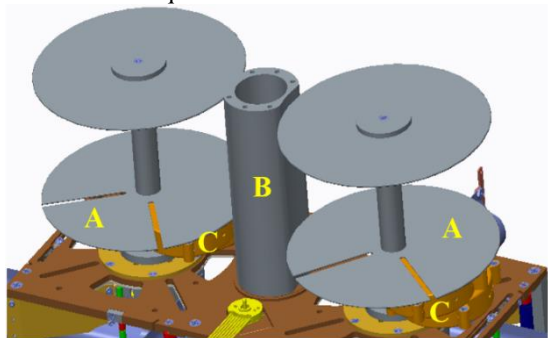


Fig. 4. Preliminary four-quadrant sail spool design for the ACS3. A: Dual-sail spools; B: Sail post; C: Two lanyard system per spool.

In order to compactly stow the booms, additional components were added to the boom deployer and removed upon completion. Fig. 5 shows the ground support equipment (GSE) used for this. An additional aluminum plate (A) with radial slots (B) is first offset from the boom deployer top plate by spacers (C). This allows radial spring-loaded (D) sliding rollers (E) to be added, which provide additional pressure to the coil during stowage to increase the packaging efficiency. During the coiling process, 0.5 mm thick shims (not shown here) are also temporarily added radially to the top and bottom plate to guarantee a more uniform final height of the coil, which ultimately reduces friction and abrasion during deployment. Hex rods (F) are then coupled to the boom spools by the hex-shaped holes of the latter. These rods act like shafts, that ultimately get manually cranked using a ratchet wrench. Reaction against the moments generated during the coiling process is provided by placing the deployer in a frame with several vertical bolts (G) accordingly spaced. Since the two boom hubs are free to rotate independently, in order to keep both steel tapes (H) tensioned during packaging, the shafts are coupled by a gear train. Sometimes, when enough friction in the system built up, as the diameter of the coil increased, the lead gear (I) slipped with respect to the trail gear (J), loosening the correspondent steel tape. It was then necessary to remove the idler gear (K) to decouple the larger gears and rotate the trailing spool the amount needed.

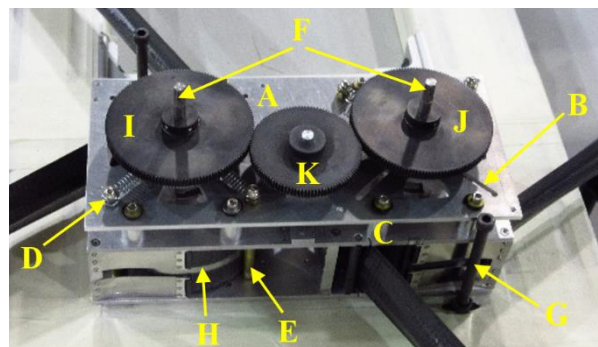


Fig. 5. Boom deployer GSE components for efficient boom packaging. A: Additional plate; B: Radial slots; C: Spacer standoffs; D: Radial linear springs; E: Radial sliding rollers; F: Hex shafts; G: Reaction frame (bolts); H: Steel strip; I: Lead gear; J: Trail gear; K: Idler gear.

4. Structural Analysis

The Mini-CTM booms were analyzed in the context of the NEA Scout mission (i.e. for a single square sail configuration) and in comparison with metallic Elgiloy TRAC⁵ booms. Under the criteria of NEA Scout, the two boom systems had similar structural performance.

Because the sail membrane tension is an important parameter for reflectivity and performance, the first goal of structural analysis was to establish a guideline for sail tension. There is a limit on the maximum sail tension that a given set of booms can maintain without buckling or taking an unacceptable shape. The second goal of the analysis was to identify the normal modes of the sail for the consideration of the attitude control team.

¹ https://glenair.com/hold_down_release_mechanism_technology/index.htm

Abaqus/Standard¹⁹⁾ is used to build a model of the sail system, shown in Fig. 6, with a detailed representation of the sail booms. The booms were each modeled with 68520 S4R shell elements and the sail membrane was modeled as a single square M3D4R membrane element.

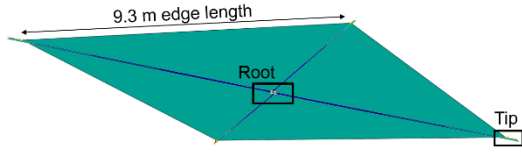


Fig. 6. A wide view of the sail system model.

The root condition included rigid models of two parts of the sail deployer: the boom spools and the sliding rollers. Contact conditions were enforced between the booms and both the spools and rollers. Additionally, a displacement condition enforced the connection between the booms and spools at two points on each boom root, as shown in Fig. 7.

At the boom tip, the connection to the sail membrane was modeled with a simple spring and a rigid body that represented the boom tip fitting. This is depicted in Fig. 8.

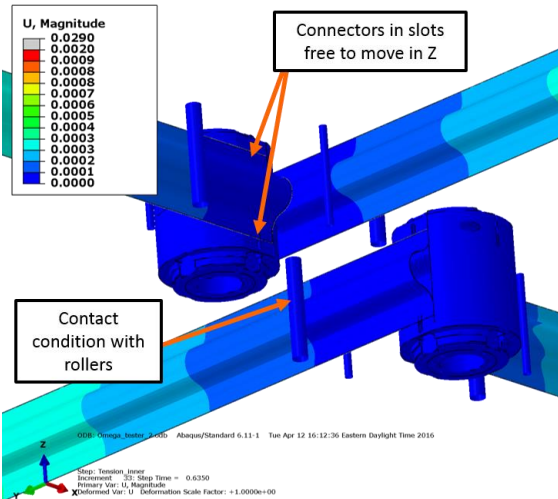


Fig. 7. The boom root conditions of the sail system model. Contact between the boom and the spools was also included in the model.

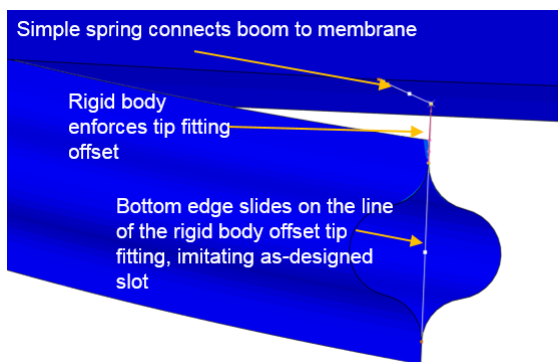


Fig. 8. The connection between the boom tip and sail membrane corners in the sail system model.

Two measures of global stiffness were used for the sail system: “windmill angle,” illustrated in Fig. 9, and out-of-plane displacement, illustrated in Fig. 10. These are simple descriptions of the sail shape that capture the way it changes in response to tensioning of the sail. Tensioning

was accomplished in the model by shortening the connector elements that link the sail corners to the boom tips.

Fig. 11 and Fig. 12 show how the sail shape changes with changes in the sail tension. Windmill angle and out-of-plane displacement both increase with increasing tension of the system, and the system becomes softer in out-of-plane displacement as tension increases. The composite mini CTM boom system was slightly softer than the metallic TRAC boom system in out-of-plane sail displacement, reflecting the lower stiffness of the composite cross-section in bending. Both boom systems provided an acceptable range of membrane tensioning, and a nominal sail tension of 1.4 N for the Mini-CTM system was selected, with analysis supporting some margin for higher tension.

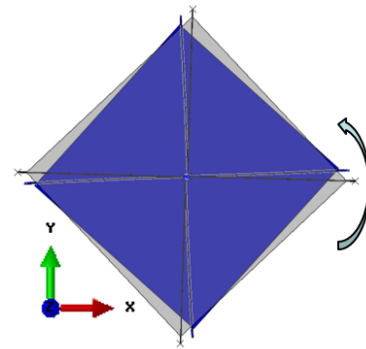


Fig. 9. Global windmill displacement/rotation of the sail system relative to the spacecraft bus.



Fig. 10. Out-of-plane displacement of the sail system relative to the spacecraft bus.

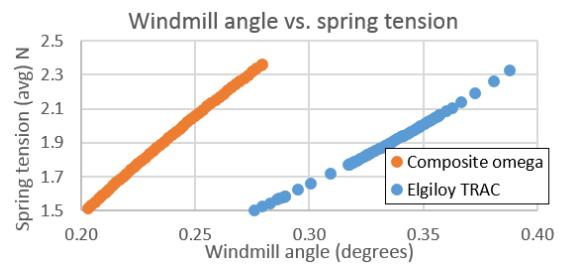


Fig. 11. Windmill displacement vs. sail membrane tensioning spring load.

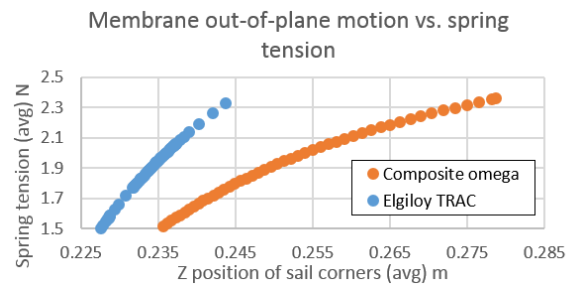


Fig. 12. Out-of-plane displacement vs. sail membrane tensioning spring tension.

Modal analysis showed that the three lowest modes of the structure are a windmilling motion, an in-plane

translation of the sail membrane, and a saddle shape. These three modes are shown in Fig. 13. There is a relationship between sail tension and the modal frequency of the sail: at a higher tension, the bent boom shape and increased out-of-plane displacement reduce the stiffness of the system in certain motions. The nominal sail tension for the Mini-CTM was 1.4 N, and 2.4 N was considered as a worst-case high tension.

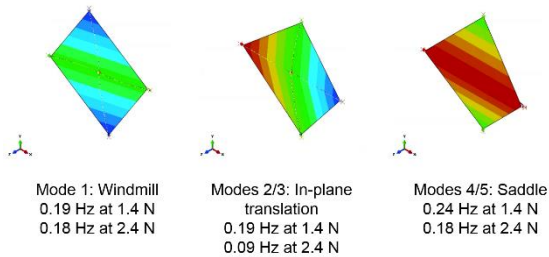


Fig. 13. The three lowest modes of the sail system. Colors correspond to out-of-plane displacements.

Thermal analysis of the Mini-CTM boom, not shown herein, supported earlier conclusions⁶⁾ that composite thin-shell booms experience far less thermal distortion than metallic booms.

5. Testing Campaign

5.1 Ground Support Equipment (GSE)

Full-scale deployment tests of the system were conducted on LaRC's large flat floor. Fig. 14 shows one of the test configuration adopted. Here, each boom tip was supported by a standalone free-floating air-bearing cradle. These units were custom-built and were designed to off-load the boom tip and keep it leveled with the boom root throughout deployment, while minimizing the bending moment at the root as a result of friction with the floor. The cradles used a 20.8 MPa Nitrogen and Oxygen filled bottle system, which required no external hoses that could interfere with the booms or sail and lead to unwanted reaction torques. Therefore, the three air bearings of each cradle were directly fed by the air bottle after the air pressure was regulated down to the appropriate input pressure of 40 psi. Up to 20 minutes of continuous operations were possible with a single bottle charge. The large triangular arrangement of the air bearings enabled a cradle design with a low CM located below the attachment point to the boom tip. The connection fixture to the boom tip was through a two-axis joint that allowed free rotation of the cradle about the vertical axis, as well as boom twist about the longitudinal axis. The cradle's CM was located near this joint so as to reduce reaction moments. Deployment proceeded as slowly as possible to minimize inertial reactions into the booms. A secondary set of four boom off-loaders, made from three dimensional (3D) printed plastic parts and a furniture slider bottom surface, came into play half-way through deployment so as to prevent the booms from sagging under gravity at their mid-point.

In addition, a central turntable permitted rotation about the vertical axis of the ACS3 as the booms extended,

although in-plane translation was constrained. To reduce free-spinning of the entire system, an 8.5 kg dummy mass block of steel, with a rotational inertia similar to that of the rest of the CubeSat, was coupled to the boom deployer.

An EDU electronic system built with Arduino²⁰⁾ components was used to control the ACS3 and acquire control parameters such as motor temperature, boom spool rotation counts, deployment progress LED lights or end of deployment signals. This system included all the functionality of a future dedicated motor controller board. This electronics unit rested atop the sail spool.

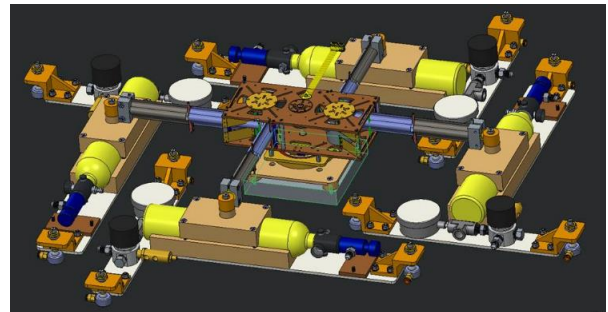


Fig. 14. Air bearing cradle configuration at the start of a boom-only deployment test. The central turntable is shown underneath the boom deployer, but the dummy mass is not omitted herein.

5.2 Functional Testing

The objective of the full-scale deployment test campaign was to demonstrate functionality of the complete boom and boom deployer system during all stages of deployment: at the beginning, where the maximum loading on the motor is expected; in the middle, where the maximum coil blossoming should occur; and at the end, where the maximum loading on the boom is expected. A secondary objective was to determine means to characterize deployment by: video recordings with small cameras at different locations, some of which that could be implemented in a future flight system; a 3D motion capture system (VICON videogrammetry system²¹⁾); and sensors feedback. The latter includes thermocouples, infrared temperature sensors, boom spools' magnetic encoders, infrared reflectance sensors for end of deployment confirmation, or motor counts (hall sensors), rotational speed and current detectors.

The test methodology consisted of, first, carrying out boom only deployments on the flat floor with an increasing degree of realism. Secondly, stretching as well a surrogate sail made from an arrangement of Kevlar[®] strings coupled with linear springs, which loaded the booms at the end of extension to approximately 2 N, in order to simulate the final sail tensioning phase.

Unfortunately, flat floor imperfections, in the form of cracks and slopes, prevented using the boom tip air-bearing cradles without any interaction with the deployer or booms during deployment. Several measures were taken to achieve realistic valid deployments with minimal manual interactions with the boom tips during deployment, and friction of boom tip off-loaders. Since the booms cannot be motor retracted given the design of the deployer, repackaging of the system was a slow task, and thus not many deployment tests were planned.

Table 1 shows the deployment test matrix carried out and the GSE configuration arrangement followed for each test. The first two tests were carried out with a fixed boom deployer (i.e. not allowed to rotate) and furniture sliders at the boom tips, as well as the boom mid-length points for the case of Test 2. These tests were successful and proved that the boom deployment mechanism worked flawlessly. For Test 3, the air-bearing cradles and the turntable were introduced (see Fig. 14). It was then, when the slopes on the “flat-floor” were discovered. Test 4 went back to using boom tip furniture sliders, but implemented the turntable and a dummy mass to minimize system rotation, and thus, lateral friction on the boom tips that could lead to buckling.

Test #	1	2	3	4	5	6	7	8
/ GSE Configuration								
Fixed Deployer	x	x				x	x	x
Turntable			x	x	x			
Dummy Mass				x	x			
Middle Furniture Sliders	x	x	x	x	x	x	x	x
Tip Furniture Sliders	x	x		x				
Air-Bearing Cradles			x		x	x	x	x
Teflon® Floor Tracks:					x	x	x	
(s) - straight; (c) - curved					(s)	(s)	(c)	
Hand-Guided	x		x					x
Sail Surrogate						x	x	x

Table 1: Full-scale deployment test plan with GSE arrangement.

In order to be able to use the air bearings, which would provide more realistic loading conditions during the critical final stage of deployment (sail tensioning), low-friction tracks made from 6 mm Teflon® rods were taped to the floor to guide the cradles. For Test 5, a straight four-lane floor track lay-out with a free-to-spin boom deployer at the center was arranged. Friction with the tracks forced the deployer to rotate, as the boom exit angle needs to change during deployment given the reduction in boom coil size and the fixed exit rollers used. For Test 6, the booms were partially re-coiled and the sail surrogate was added. This was the first sail-like tensioning test and only consisted of extending out the booms 30 cm until the springs loaded them appropriately. For Test 7, the deployer was fixed, and thus, curved floor tracks were laid-out to account for the continuous change in boom tip direction, as shown in Fig. 15 points of the ideal curves were determined with computer aided design (CAD) tools and marked on the floor, with the aid of laser, prior to taping the flexible Teflon® rods. This test was the first end-to-end deployment test, but required interaction with the cradles due to them catching on floor and track defects. For the last test (#8), the floor tracks were removed and the cradles were manually redirected to the correct path once they started drifting due to the floor slopes and cracks.

As a result of the various successful tests, it was determined that the deployment mechanisms and booms performed well during all phases of deployment, and that the booms could be loaded to the required levels. Therefore, it was concluded that continuing to battle an imperfect floor to achieve an ideal set of boundary

conditions was not deemed necessary at that point, and thus further testing would resume when the flat floor was repaired or another similar facility would be available.

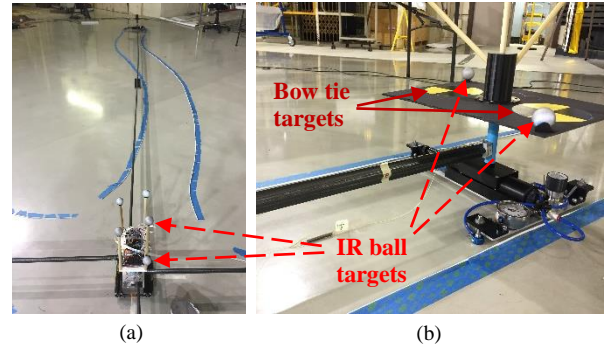


Fig. 15. (a) Boom deployer view of deployment Test 7 with the curved floor tracks; (b) Boom tip air-bearing cradle inside the floor track showing several infrared (IR) markers and the bow tie targets.

Fig. 16 shows the motor feedback parameters obtained during Test 5. The motor angular velocity input profile adopted consisted of a three step function: the initial 10% of the motor counts (deployment) at a 3000 rpm speed; the following 80% at 7500 rpm; and the final 10% at 3000 rpm, so as to not overload the motor during the critical stages of deployment (start and end). For all deployment tests, the motor torque margin was always ≥ 2 , as the maximum current observed was approximately 0.5 A, and the maximum allowed by the motor is 1 A. As can be seen from the graph, the motor current reduces over time from 0.3-0.35 A to 0.2 A, since friction inside the deployer reduces as the size of the boom coil diminishes. The current spike at the end of deployment, that reaches up to 0.5 A, is due to tensioning the sail surrogate. Lower current values were obtained on subsequent tests as the boom packaging efficiency was improved with the redesigned metallic GSE shown in Fig. 5. The exact motor counts for this particular test were 94294, which translates to about 255 turns of the tape spool or about 30.5 turns of the boom spools.

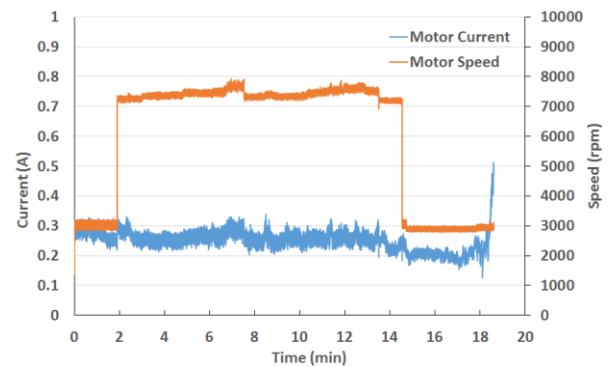


Fig. 16. Test 5 deployer motor performance.

Deployment Rate Tracking

The deployment trajectories of the four air-bearing cradles connected to the boom tips and motion of the boom deployer were measured using videogrammetry equipment. This technique provides simultaneous motion knowledge of several targets as they deploy. The Vicon® system with a set of eight Bonita B3 cameras shooting at 240 frames-

per-second was used with the Vicon® Tracker 3.2 data acquisition and post-processing software package. The arrangement of the cameras was such that, at least, three could track each boom tip throughout deployment. Each air-bearing cradle and the electronic board atop the boom deployer were equipped with five 25 mm diameter retroreflective infrared (IR) markers in a random 3D arrangement created by different length wooden sticks fixed to the targets. The centroid of the different 3D objects created by the IR markers was then tracked by the IR cameras, providing all six degrees of freedom displacements (three translations and three rotations). Linear and angular velocity and acceleration of the targets are also readily available by a simple time derivate of position knowledge. Additional bow tie sticker targets were added to the cradles to provide a less accurate redundant two dimensional (2D) motion tracking system by an overhead optical camera that took pictures every 5 seconds (photogrammetry). Fig. 15 shows some of the different targets at the boom deployer and at a boom tip air-bearing cradle.

Fig. 17 presents the translation, T, of the boom tip in all three axes during Test 3 for Boom 1 and Boom 2, which were aligned with the +Y and -X global axes, respectively. It is shown that boom deployment speed was not constant, which is in line with the motor rotation stepped profile adopted. As expected, it was a 2D planar deployment with negligible Z axis translation (T_z remains constant).

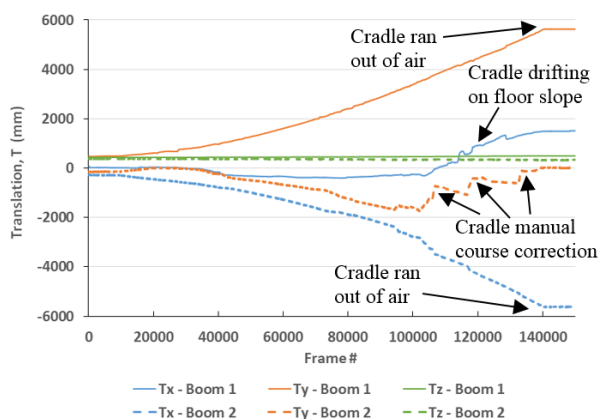


Fig. 17. Test 3 boom tip motion for Boom 1 (+Y) and Boom 2 (-X).

It can also be seen that floor defects prevented a nominal deployment, as it required half-way through the test, several manual interventions in the +Y direction to correct the course of Boom 2. This example is presented to showcase that boom tip position data can be useful to track causes of deployment anomalies, and, in this case, even evaluate floor topography. This was a shorter than usual test, in part initially devised to assess the run time of the air-bearing cradles. As shown, the bottles ran out of gas prematurely stopping the test about 0.9 m from the end of deployment planned. The air bearing input pressure was then reduced for future tests, from the nominal 60 psi to an experimental minimum working pressure of 40 psi, in order to extend the run time of the units and enable at least 20 min long tests. Slowing the deployment process reduces inertial effects and dynamics, as well as motor loading, so

it is advisable. The real in-space operation might even proceed slower than this, if deemed necessary.

Fig. 18 shows the boom deployer rotation about the out-of-plane Z axis during Test 4. As the motor and boom spools rotate in a clockwise (+Z) manner and the whole system is free to spin on a turntable (simulating the in-space condition), the reaction torque causes the system to spin counter-clockwise. This is evident from the graph, where the R_z rotation angle decreases over time. During extension, the boom tips follow a curve similar to that shown in Fig. 15 (a), with a counter-clockwise spiral motion until the very last stages where the curvature changes to a clockwise motion. However, lateral friction of the furniture slider off-loaders with the floor causes a momentum build-up at the boom root. In Fig. 18, the abrupt -30° rotation observed is caused by the deployer system self-aligning with the new boom tip direction following the principle of minimum energy. The change in spin direction at the end of deployment, when the boom roots fully develop and lock into place, produces a clockwise rotation of about $+17^\circ$, with a final total rotation of $+10^\circ$ as the deployer settles. Knowledge of the relative motion of the spacecraft hub with respect to the unfurling solar sail is important to avoid boom root buckling during deployment, as well as to size the controller that will need to dampen any unwanted remaining rotational rates of the sailcraft following deployment.

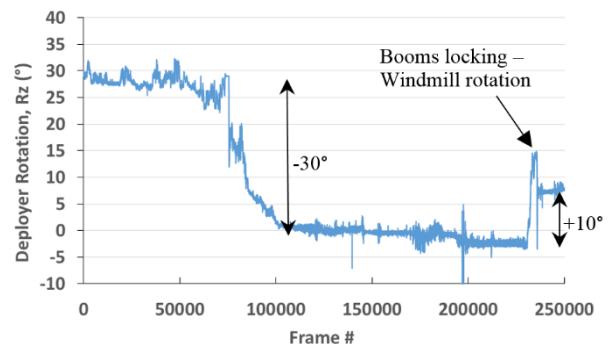


Fig. 18. Test 4 boom deployer rotation about the vertical Z axis.

5.3 Environmental Testing

The environmental testing campaign carried out on the CS3 unit was conceived in the context of the NEA Scout mission. Four main tests were carried out: vibration testing following the Exploration Mission 1 (EM-1) preliminary launch load environment of the Space Launch System (SLS) with subsequent post-vibe complete boom deployment; Thermal (cold) - vacuum acceptance test of the deployer motor and tape heater units alone; Partial boom-only deployment test under thermal (hot) and vacuum conditions; Partial boom-only deployment testing under thermal (cold) and vacuum conditions with subsequent ambient complete boom deployment.

Vibration Test

The objective of the vibration test was to assess the survivability of the CS3 sub-unit, which included the boom deployer, full-scale coiled booms, and the sail spool with a dummy folded/rolled single-square Mylar® sail, to the expected launch environment. Visual inspections between

each test axis included: fastener loosening, changes in boom coil diameter, changes in clearances between boom coils and the top/boom deployer plates, configuration of the locking mechanism, loosening of bearings, loosening of the motor, disengagement or misalignment between drive gears, and any other visible damage.

Fig. 19 shows the test configuration adopted for the Z axis vibration tests. Two triaxial control accelerometers were mounted to the upper and lower fixture steel blocks and used as feedback to the shaker controller. These heavy blocks are used to stiffly secure the CS3 unit to the 30 cm magnesium block, that ultimately bolts down to the shaker table. Two triads of single-axis response accelerometers (ACC1 and ACC2) oriented in the principal X, Y and Z axes were fixed to the upper and lower plates inside the deployer.

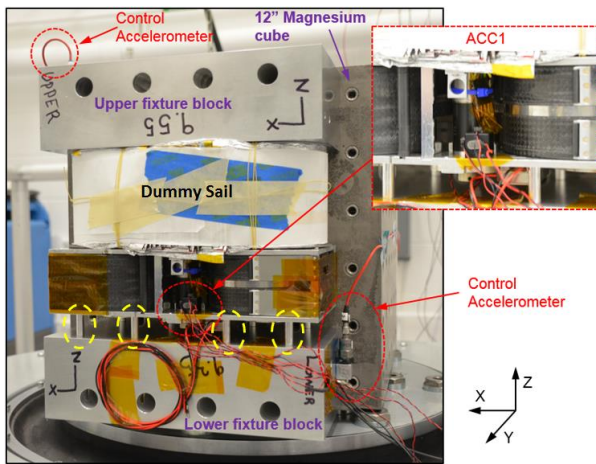


Fig. 19. Z axis vibration test setup showing the location of the two controls and one of the response (ACC1) accelerometers. The yellow dashed line ellipses show the lower fixture block standoffs.

Table 2 shows the vibration test matrix followed. The Maximum Predicted Environment (MPE) for the random vibration testing implemented, in terms of acceleration spectral density (ASD) was:

- 0.1 g^2/Hz in the 20-100 Hz range.
- Ramp down to 0.04 g^2/Hz at 150 Hz.
- 0.04 g^2/Hz in the 150-500 Hz range.
- Ramp down to 0.01 g^2/Hz at 2000 Hz.

This adds up to 7.2 g_{rms} , and 10.1 g_{rms} for the MPE +3dB levels actually used.

Axis	Test	Level	Duration/Rate
Z, X, Y (repeated for all 3 axes)	Signature Sine Sweep	0.25 g_{pk}	4 octave/min
	Random Vibration (MPE +3dB)	10.1 g_{rms}	3 min
	Signature Sine Sweep	0.25 g_{pk}	4 octave/min
	Visual Inspection	N/A	N/A
N/A	Deployment Test	N/A	N/A

Table 2. Vibration test matrix with the levels and durations/rates used.

The stowed CS3 unit showed no signs of visible damage or alteration during vibration testing. Fig. 20

shows, as an example, the Z axis random acceleration spectral input and the response of two uniaxial accelerometers in that same axis. Pre and post-vibration sine sweeps showed small differences at mid/high frequencies due to the loosening of the lower fixture block mounting standoffs/screws. Fig. 21 shows the Y axis sine sweep input and response of the ACC1-Y accelerometer. It can be seen that the first pre-vibe global mode at ~450 Hz split into two modes after the Y axis random vibration test. This is probably due to some flexibility induced in the test unit that allowed the top part to move with respect to the bottom part. Some other smaller variations at higher frequencies are also evident. The location of these standoffs/screws is shown in Fig. 19. These components do not form part of the CS3 unit and are just there to offset the deployer from the fixture block in order to clear off some of the protruding deployer elements. These series of development vibration tests will be redone once the final SLS's MPE loads are available. Proper fixing of the lower fixture block through stiffer connectors will also be guaranteed.

The post-vibration boom only deployment test proceeded nominally on all fronts with no signs of damaged or displaced components. The motor current output data were also nominal.

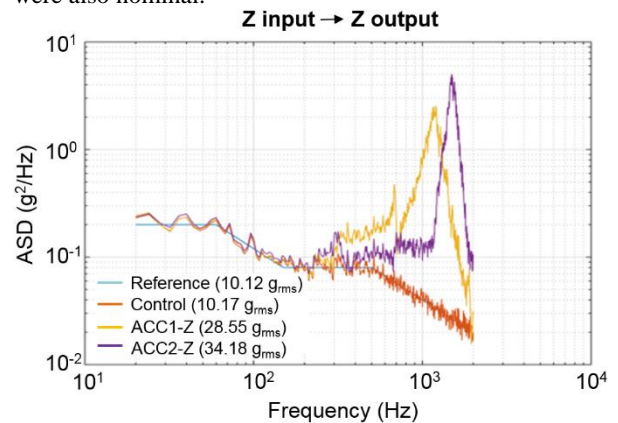


Fig. 20. Z axis random vibration spectral input and response of the ACC1-Z and ACC2-1 accelerometers.

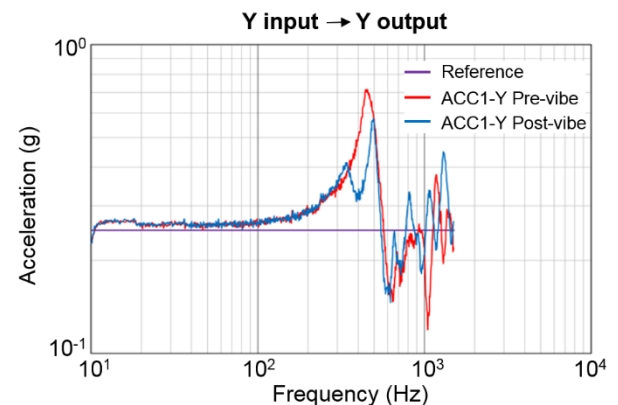


Fig. 21. Y axis sine sweep input and response of the ACC1-Y accelerometer before and after the Y axis random vibration test.

Thermal-Vacuum Test: Deployer Motor & Heater

A development thermal-vacuum (TVAC) cold test on the deployer motor and heater was conducted to gain confidence on the components prior to testing the complete

CS3 unit. Individual cold functioning tests without cycling were recommended by project thermal engineers. A small TVAC bell jar was used for the test. The test setup, fixture and thermocouple (TC) locations are depicted on Fig. 22. Very low pressures of $< 2.6E-4$ Pa were achieved prior to ramping down in temperature. The brushless DC motor was soaked to -50 °C and -70 °C. Then successfully heated with the space-rated Kapton® film tape-heater to its minimum recommended operating temperature of -30 °C, and successfully operated for 20 min (expected deployment run time with 10% margin), while keeping the temperature within the desired ± 5 °C limit using the tape-heater. As the motor shaft was free to spin there was no motor loading.

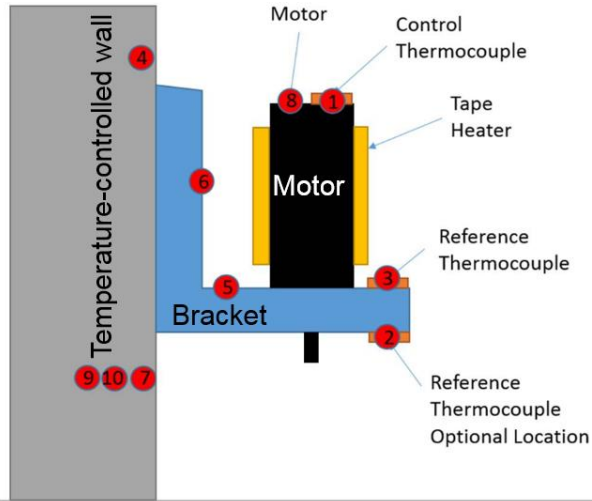


Fig. 22. Deployer motor/heater TVAC test setup with TC locations.

Fig. 23 shows the temperature profile graphs obtained during the test at the control TC and the motor TC. Given the small contact area between the motor and the bracket, the temperature of the latter needed to be driven well below the desired one for the motor. From the graph, it is evident how the temperature cycled between the acceptable limits during the motor operation phase. The tape-heaters draw 7 W of constant power during operation (10 V and 0.7 A), which stayed within the power budget established for NEA Scout.

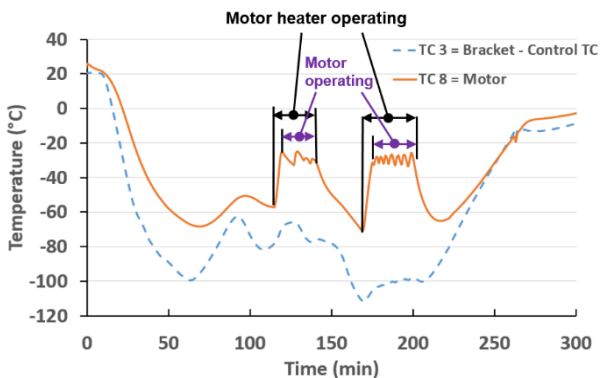


Fig. 23. Temperature-Time curves of the motor/heater cold TVAC test without motor loading.

The deployer motor showed no signs of damage during the TVAC test and was confirmed to be ready for integration into the CS3 unit for complete TVAC testing. A comparison between this no-motor-load cold TVAC test

and another one carried out under ambient conditions (101.3 kPa, and $+20$ °C) showed a motor efficiency drop of 2-2.5 for the lower limit of the defined operating temperature range, which was measured as a relative motor current ratio. This suggested that it would still be acceptable to run the motor for the complete TVAC test at -30 °C. However, since operating the motor at a higher temperature was not restricted from a power consumption standpoint, a different future operational lower limit could be chosen if needed.

Thermal-Vacuum Testing: CS3 Unit

Following NEA Scout's environmental test plan, the CS3 unit was functionally tested under hot ($+70$ °C) and cold (-70 °C) vacuum conditions. Single temperature soaks without cycling were followed as recommended by project thermal engineers. A 1.8 m diameter and 1.8 m long cylindrical TVAC chamber was used for the test. Partial boom only deployments inside the chamber to a boom length of 0.5 m were used to test the validity of the system in the space environment, as the most challenging phase for the deployer mechanism is the first stages of deployment where system friction is at its maximum. The motor rotational speed was reduced to a constant velocity of 825 rpm in order to simulate the 20 min of operating time of a full deployment, given the boom extension length constraint imposed by the size of the chamber. The motor was successfully operated in high-vacuum ($< 1.3E-4$ Pa) for 20 min at $+70$ °C after a 1 h soak at this temperature. Fig. 24 shows the motor performance under hot thermal-vacuum ($+70$ °C) conditions during a functional test that consisted of initially deploying all four full-scale 6.85 m coiled booms by 0.5 m. A small motor temperature increase of about 3.5 °C over the duration of the test was observed due to operation of the motor in vacuum. The motor current readings were below 0.2 A, reflecting that the motor and deployer system perform best at elevated temperatures (compare this with Fig. 16).

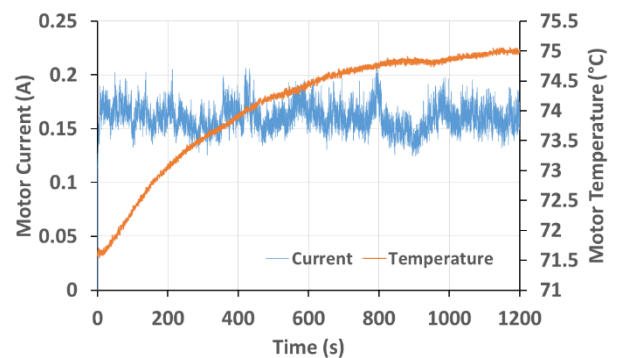


Fig. 24. Motor performance under hot TVAC ($+70$ °C) conditions during a partial booms-only deployment test.

After the hot test, the chamber was opened and the booms were packaged again. The cold TVAC test then proceeded as follows:

- Ramped up at a maximum of $3^{\circ}\text{C}/\text{min}$ from room temperature ($+20$ °C) to $+70$ °C.
- Soaked for 1 hour at $+70$ °C ± 1.5 °C to outgas any volatiles.

- Ramped down at a maximum of 3°C/min to -70 °C.
- Soaked for 1 hour at +70 °C ± 1.5 °C.
- Ran the motor heaters to bring up the motor temperature to -30 °C, stabilizing it to within ± 5 °C.
- Deployed the four coiled 6.85 m booms by 0.45 m in 17 min.

Fig. 25 shows the motor and motor heater performance under cold thermal-vacuum (-70 °C) conditions during a partial booms-only deployment test. The motor rotational speed was further reduced to a constant velocity of 775 rpm to simulate approximately 20 min of run time for a full deployment. As shown, the motor was successfully operated for 17 min, just a little short of the target, due to one boom tip catching on a thermocouple wire. This was observed in real time by the video camera held inside the TVAC chamber. Deployment was then stopped remotely so as to not damage the boom. On the whole, the test was considered successful given the deployer performance trend observed. Fig. 25 evidences that the motor heater and its controller were capable of bringing up the motor temperature to the desired -30 °C and hold it within ± 5 °C by cycling the heater on and off, including system lagging. As expected, the performance of the motor in the cold conditions dropped. The motor current reached a maximum of 0.6 A momentarily, but in general was lower than 0.5-0.55 A. The current is expected to decrease further as deployment progresses. These test results provide confidence that this motor and heater combination could be used for flight with enough motor torque margin, even at the motor minimum operating temperature limit of -30 °C ± 5 °C defined.

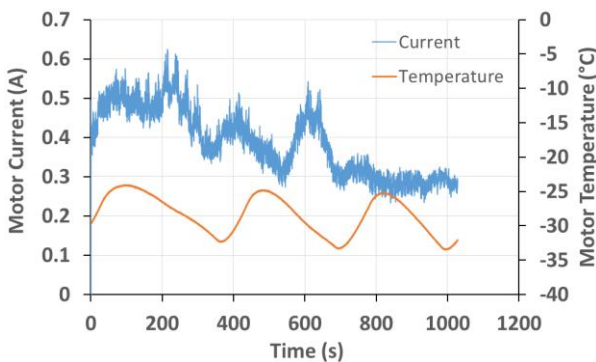


Fig. 25. Motor and motor heater performance under cold TVAC (-70 °C) conditions during a partial booms-only deployment test.

The commercial-off-the-shelf (COTS) brushless DC Maxon²²⁾ motor with added high-vacuum rated Braycote[®] 601E grease lubricant showed no signs of damage during the TVAC testing campaign and could be considered for a flight ACS3 unit. The final full-scale post-TVAC deployment test under ambient conditions, that essentially completed the rest of the partial deployment test of the cold TVAC test, was nominal. The test configuration was similar to that of Test 8 shown in Table 1 and was carried out on the same flat floor.

6. Conclusions

A summary of the design and development of NASA LaRC's new Advanced Composites-based Solar Sail System (ACS3) for future small satellite science and exploration missions has been presented. The ultra-lightweight scalable rollable booms made from state-of-the-art thin-ply composite materials enables a scalable solar sail design that can achieve a 10% higher characteristic acceleration than current 6U CubeSat solar sail designs, such as NEA Scout. Such a system will be a faster and more agile (less rotational inertias) sailcraft, that can extend the capabilities of these relatively low-cost and small solar sails.

The boom deployer uses a novel "puller" type concept to drive the booms, aimed at minimizing the known issue of coil blossoming by design. A system of retractable lanyards is introduced at the sail spools to yield a near constantly-tensioned four-quadrant sail through all mission phases. Removable GSE was designed to achieve very high boom packaging efficiencies of about 85%, in order to fit all four 6.85 m booms in the small volume available.

The structural analysis of the fully integrated solar sail showed that, as for the case of a similar sail tensioned by an Elgiloy TRAC boom system, the Mini-CTM composite boom system provides an acceptable range of membrane tensioning. The analysis predicts at least a 70% safety margin over the nominal sail tension of 1.4 N adopted. Modal analysis showed that the lower frequencies of the tensioned sail system are within an acceptable limit, which could be established at around 0.09-0.1 Hz, even for the higher sail tensioning worse-case of 2.4 N. A thermal analysis at boom component level, not shown herein, also supports the conclusion that the composite boom experiences far less thermal distortions than equivalent and similar metallic booms, and is thus not a future mission risk any more.

The ambient functional testing campaign of the boom system, with a surrogate sail made with Kevlar[®] strings and linear springs to simulate final sail tensioning, showed the challenges of deploying on the ground such a gossamer structure, particularly when working with an imperfect "flat floor". Given the various successful tests with minimal manual interaction with the booms, it was determined that the booms and deployer performed well, and that the booms could be loaded at the end to the required levels. A 3D videogrammetry system was successfully used to track the deployment rates (i.e. boom tip displacement, speed and acceleration, and deployer rotation, angular velocity and acceleration), and help capture causes of deployment anomaly. A final windmill rotation of the system due to the booms locking into position was observed and will need to be evaluated by the future attitude control team, which will need to dampen the resultant angular rates of the sailcraft.

The CS3 unit survived the vibration testing campaign without any signs of damage and the post-vibration deployment test was nominal. However, some loosening of GSE screws resulted in small differences in the mid/high frequency between the pre and post-vibration sine sweeps.

Thermal-vacuum tests at hot (+70 °C) and cold (-70 °C) conditions, that consisted of partial booms-only

deployments inside the TVAC chamber, showed that the various CS3 mechanisms, sensors, booms, deployer motor and motor tape heater worked flawlessly. As expected, the deployer motor performance dropped while running at its recommended minimum operating temperature, but the motor torque margin found is still acceptable.

All in all, the CS3 unit is ready to be part of an actual mission and serve as the propellantless propulsion system of a CubeSat-based sailcraft. Nonetheless, the ACS3, that will use a four-quadrant sail configuration and slightly taller 55-60 mm Mini-CTM/Omega booms (see Fig. 2), would be the preferred future choice for a solar sail technology demonstration mission. A current effort is also examining scaled-up versions of the ACS3 for higher performance and more capable solar sails systems aboard small satellite platforms that would extend their usefulness. For example, a preliminary design of a ~360 m² sail area ACS3 to be housed on a 12U CubeSat platform is presently being studied by the LaRC team for possible near-to-mid-term implementation. This solar sail spacecraft could achieve a characteristic acceleration of ~0.15 mm/s² at 1au. Such a system would use larger 14 m class CTM/Omega composite booms and four scaled-up boom deployers, which are currently being developed under a parallel effort as part of a Game Changing Development Program (GCDP) project called “Deployable Composite Booms” funded by the NASA Space Technology Mission Directorate (STMD).

Acknowledgements

This work is financially supported by NASA’s Advanced Exploration System (AES) Program under the Future Exploration Projects portfolio. The help from past NASA interns, Charles White, Matthew Lee, David Shekhtman, and Wayne Page, as well as from the composite fabrication technicians, Jacob Tury and Kevin McLain, is gratefully acknowledged.

References

- 1) Alhorn, D., et al., *NanoSail-D: The Small Satellite That Could*, 25th Annual AIAA/USU Conference on Small Satellites, Logan, Utah, 2011, SSC11-VI-1.
- 2) Bidy, C., Svitek, T., *LightSail-1 Solar Sail Design and Qualification*, 41st Aerospace Mechanisms Symposium, Pasadena, California, 2012.
- 3) Ridenoure, R., et al., *LightSail Program Status: One Down, One to Go*, 29th Annual AIAA/USU Conference on Small Satellites, Logan, Utah, 2015, SSC15-V-3.
- 4) McNutt, L., et al., *Near-Earth Asteroid Scout*, AIAA SPACE 2014 Conference and Exhibition, San Diego, California, 2014, AIAA 2014-4435.
- 5) Banik, J.A., Murphey, T.W., *Performance Validation of the Triangular Rollable And Collapsible Mast*, 24th Annual AIAA/USU Conference on Small Satellites, Logan, Utah, 2010, SSC10-II-1.
- 6) Stohlman, O., Loper, E. R., *Thermal Deformation of Very Slender Triangular Rollable and Collapsible Booms*, 3rd AIAA Spacecraft Structures Conference, San Diego, California, 2016, AIAA 2016-1469.
- 7) Fernandez, J.M., *Advanced Deployable Shell-Based Composite Booms For Small Satellite Structural Applications Including Solar Sails*, 4th International Symposium on Solar Sailing, Kyoto, Japan, 2017.
- 8) Rennie, B.B., *New Closed Tubular Extendible Boom*, 2nd Aerospace Mechanisms Symposium, ed: Herzl, G.G., JPL, TM 33-355, pp 163-170, 1967.

- 9) Herbeck, L., et al., *Development and Test of Deployable Ultra-Lightweight CFRP-Booms for a Solar Sail*, European Conference on Spacecraft Structures, Materials, and Mechanical Testing, Noordwijk, The Netherlands, 2000.
- 10) Hillebrandt, M., et al., *The Boom Design of the De-Orbit Sail Satellite*, 13th European Conference on Spacecraft Structures, Materials and Environmental Testing, Braunschweig, Germany, 2014 (ESA SP-727, June 2014).
- 11) Hoskin, A., *Blossoming of Coiled Deployable Booms*, 56th AIAA/ASME/ASCE/AHS/ASC Structures, Structural Dynamics and Materials Conference, Kissimmee, Florida, 2015. AIAA 2015-0207.
- 12) Fernandez, J.M., et al., *Design and Development of a Gossamer Sail System for Deorbiting in Low Earth Orbit*, Acta Astronautica, Vol. 103, 204-225, 2014.
- 13) Fernandez, J.M., et al., *Deployment Mechanisms of a Gossamer Satellite Deorbiter*, 15th European Space Mechanisms & Tribology Symposium, Noordwijk, The Netherlands, 2013.
- 14) Sobey, A.R., Lockett, T.R., *Design and Development of NEA Scout Solar Sail Deployer Mechanism*, 43rd Aerospace Mechanism Symposium, Santa Clara, California, 2016.
- 15) Stohlman, O., Fernandez, J.M., et al., *Testing of the DeOrbitSail Drag Sail Subsystem*, 54th AIAA/ASME/ASCE/AHS/ASC Structures, Structural Dynamics and Materials Conference, Boston, Massachusetts, 2013. AIAA 2013-1807.
- 16) Meyer, S., Hillebrandt, M., et al., *Design of the De-Orbit Sail Boom Deployment Unit*, 13th European Conference on Spacecraft Structures, Materials and Environmental Testing, Braunschweig, Germany, 2014.
- 17) Fernandez, J.M., et al., *CubeSail: A Low-Cost Nano-Solar Sail for Space Debris Reduction in LEO*, 1st IAA Conference on University Satellite Missions, Rome, Italy, 27-29 January 2011.
- 18) Lappas V.J., et al., *CubeSail: A Low-Cost CubeSat Based Solar Sail Demonstration Mission*, Advances in Space Research, Vol. 48, Issue 11, 1890-1901, 2011.
- 19) Abaqus v. 6.13-3, Dassault Systèmes Simulia Corp., Providence, RI, USA.
- 20) Arduino, www.arduino.org
- 21) Vicon, www.vicon.com
- 22) Maxon, www.maxonmotorusa.com